Journal of Photochemistry and Photobiology A: Chemistry 215 (2010) 81–89

Contents lists available at ScienceDirect

Journal of Photochemistry and Photobiology A: Chemistry

journal homepage: www.elsevier.com/locate/jphotochem

Irradiance modeling in annular photoreactors using the finite-volume method

J. Esteban Duran, Fariborz Taghipour, Madjid Mohseni*

Department of Chemical and Biological Engineering, The University of British Columbia, 2360 East Mall, Vancouver, BC, Canada V6T 1Z3

ARTICLE INFO

Article history:
Received 21 January 2010
Received in revised form 19 July 2010
Accepted 22 July 2010
Available online 30 July 2010

Keywords:
CFD
UV photoreactor
Radiation field
Lamp emission model
Irradiance
Photocatalysis

ABSTRACT

A computational radiation field model for simulating the irradiance in single-phase annular photoreactors was developed and evaluated experimentally. The developed model included the lamp within the computational domain allowing to incorporate important interactions between the UV radiation, the quartz walls, and the Hg vapor inside the lamp. Several lamp emission models were evaluated against far- and near-field experimental data. The models with diffused radiation emission showed better overall irradiance prediction capabilities. In particular, a modification of the extensive source volumetric emission model that incorporates the high photon absorbance/re-emission effect produced by the Hg vapor in the lamp illustrated superior results. This latter model showed excellent agreement with near- and far-field experimental data indicating its suitability for integration in multi-physics models for the simulation of photoreactor performance. The advantages of this model are: it is very easy to set up; it comprises the main physical phenomena occurring in the lamp; and it allows for taking into account important lamp-sleeve interactions. Experimental results reaffirmed the importance of applying proper estimates of the lamp power output under the actual operating conditions to perform accurate simulations of radiation distribution.

1. Introduction

The use of photoreactors in water treatment applications has increased substantially over the past few years. They are commonly employed in ultraviolet (UV) disinfection and UV-based advanced oxidation processes (AOPs). A particularly emerging and promising AOP is heterogeneous photocatalysis [1–3]. Photocatalytic oxidation processes involve the use of semiconductor photocatalyst materials, predominantly titanium dioxide (TiO_2), activated by UV irradiation. One major configuration of photocatalytic reactors has the catalyst immobilized in layers to reactor inner surfaces. Since the degradation rate of contaminants in these immobilized photocatalytic reactors is directly dependent on the UV irradiance at the photocatalyst surface, the radiation field (photon distribution) within the reaction volume is one of the critical factors that determine the overall conversion and photoreactor performance. In this sense, when modeling immobilized photocatalytic reactors, the accurate prediction of the radiation field (and consequently the UV irradiance on the catalyst-coated surface) is of paramount importance.

Modeling the radiation field in a given photoreactor involves solving the radiative (photon) transfer equation (RTE) [4,5]. For monochromatic radiation, the RTE is defined as:

$$\frac{dI(\vec{r},\vec{s})}{ds} + (\kappa+\sigma)I(\vec{r},\vec{s}) = j^e(\vec{r}) + \frac{\sigma}{4\pi}\int_{4\pi} I(\vec{r},\vec{s}')p(\vec{s}'\rightarrow\vec{s})\,d\Omega' \quad (1)$$

where I is the photon radiance, $\vec{r}$ is the position vector, $\vec{s}$ is the propagation direction vector, s is the path length, κ is the absorption coefficient, σ is the scattering coefficient, j^e is the emission (source) term, p is the phase function for the in-scattering of photons, and Ω' is the solid angle about the scattering direction vector $\vec{s}'$. In Eq. (1), the left-hand side terms represent the radiance change along the path length s, and the loss due to absorption and out-scattering. The right-hand side terms correspond to the radiance source and the gain in radiation radiance due to in-scattering. An analytical solution for this integro-differential equation is only possible for very simple cases [6]; for most practical engineering applications a numerical approach is necessary [7].

Several numerical methods have been developed for solving the RTE. Carvalho and Farias [7] presented a review of some of these methods. Among the proposed methods, three of them have been mostly utilized and studied in the simulation of photoreactors: the Monte Carlo (MC) method, the discrete ordinate (DO) method, and the finite-volume (FV) method [8]. In particular, the FV method has been gaining much acceptance due to very favorable characteristics. In the FV method, the RTE is integrated over both the control angle and the control volume [9], which allows for conserving radiant energy and easily incorporating the method in computational

* Corresponding author. Tel.: +1 604 822 0047; fax: +1 604 822 6003.
E-mail address: mmohseni@chbe.ubc.ca (M. Mohseni).

1010-6030/$ – see front matter © 2010 Elsevier B.V. All rights reserved.
doi:10.1016/j.jphotochem.2010.07.027

Nomenclature

$C_{Fe^{2+}}$	molar concentration of Fe^{2+} (mol L^{-1})
d_o	external tube outer diameter (m)
E	radiation irradiance (W m^{-2})
ESDE	extensive source superficial diffuse emission model (refer to Table 1)
ESVE	extensive source volumetric emission model (refer to Table 1)
ESVEA	modified ESVE model that accounts for photon absorption/re-emission in the lamp plasma
ESVERA	modified ESVEA model that accounts for radiation reflection, refraction and absorption at the lamp quartz envelope
ESDER	modified ESDE model that accounts for radiation reflection, refraction and absorption at the lamp quartz envelope
ESVER	modified ESVE model that accounts for radiation reflection, refraction and absorption at the lamp quartz envelope
I	photon radiance (W m^{-2} sr^{-1})
j^e	emission (source) term (W m^{-3} sr^{-1})
L	lamp arc length (m)
LSDE	line source diffuse emission model (refer to Table 1)
LSDER	modified LSDE model that accounts for radiation reflection, refraction and absorption at the lamp quartz envelope
LSSE	line source spherical emission model (refer to Table 1)
LSSS	line source spherical sources model (refer to Table 1)
MPSS	multiple point source summation model (refer to Table 1)
MSSS	multiple segment source summation model (refer to Table 1)
n	refractive index (dimensionless)
p	phase function for the in-scattering of photons (dimensionless)
P	power output of the lamp (W)
$\vec{r}$	position vector (m)
R	distance from center of lamp to the detector (m)
$\vec{s}$	propagation direction vector (m)
s	path length (m)
$\vec{s}'$	scattering direction vector (m)
t	irradiation time (s)
T	absolute temperature of the medium (K)
V_T	total volume of actinometric solution (L)
w	irradiated window width (m)
x	axial coordinate (m)
y	normal distance from the lamp center (m)

Greek letters

α	half angle subtended by the lamp at the sensor position (rad)
θ	angle from the normal axis of the lamp (rad)
κ	absorption coefficient (m^{-1})
σ	scattering coefficient (m^{-1})
σ_{S-B}	Stefan–Boltzmann constant (5.672×10^{-8} W m^{-2} K^{-4})
Φ	quantum yield of potassium ferrioxalate at 254 nm (mol einstein^{-1})
Ω	solid angle about the propagation direction (sr)
Ω'	solid angle about the scattering direction vector $\vec{s}'$ (sr)

fluid dynamics (CFD) simulations. CFD is a very attractive modeling approach since it allows an integrated analysis of photoreactors through simultaneous modeling of hydrodynamics, species mass transport, chemical reaction kinetics, and photon flux distribution. Even though the FV method has been used in many CFD-based studies [8–14] few of them involved experimental evaluation of the radiation field simulations [13,14].

A key component in the development of a radiation field model is the definition of the lamp emission model (i.e., how UV radiation is emitted by the lamp). Several conceptual and mathematical models have been proposed in the literature [8,15–20]. A list with some of the lamp emission models most commonly employed in photoreactor modeling is given in Table 1. Imoberdorf et al. [15] recently proposed a more exhaustive lamp emission model that includes the reflection and refraction effects on/in the quartz envelope, so as the photon absorption/re-emission by the mercury vapor inside the lamp. The model was applied to the simulation of multi-lamp, homogeneous photoreactors, showing good agreement with the experimental data.

All the lamp emission models mentioned so far have been experimentally evaluated for lamps running in air, or inside homogeneous photoreactors [15–17,21,26–28]. Nonetheless, the radiation model evaluation close to the lamp (which is likely to be the location of the photocatalyst in the case of immobilized reactors) has been particularly challenging. Most studies utilized either a UV radiometer or a chemical actinometer for performing the irradiance/fluence rate measurements. Radiometers, however, are not reliable for measuring irradiance in close proximity to the radiation source, mainly due to the geometry and the variable response of the photometer within a nonparallel radiation field [29]. On the other hand, under high radiation fluxes, some actinometers can experience saturation of the reacting solution due to diffusional resistance effects. This phenomenon has been reported, for example, for the iodide/iodate actinometer for 254 nm radiation [17,28,30].

Another shortcoming of some evaluation studies is related to the estimation of the radiation output of the lamp under the working (experimental) conditions. In many cases, the lamp output was measured while running the lamp in air at ambient temperature. However, experiments were conducted with the lamp inside a reactor, enclosed in a quartz sleeve, and submerged in water at another temperature. Hence, the radiation outputs of the lamp during the experiments were likely different. For low-pressure mercury (Hg) lamps, fluctuations of 10 °C in the lamp temperature can produce changes in the emission efficiency as high as 50% [31–33]. In this sense, new measurement methods that address this issue have been recently proposed [34].

This investigation has focused on developing an FV-based model for predicting the irradiance inside single-phase annular photoreactors. The model is primarily intended to be applied to the CFD simulation of immobilized photocatalytic reactors. In the developed model, the UV lamp (monochromatic) is part of the computational domain. Hence, the reflection, refraction, and absorption of radiation at the air/quartz/water interface, as well as the absorption and re-emission of photons by the lamp plasma, could be considered. For defining an appropriate emission model for the lamp, several lamp emission models were evaluated against far-field (measuring position located away from the lamp) and near-field (measuring position close to the lamp) experimental data. The employed measurement techniques aimed to eliminate the previously discussed errors associated with irradiance determinations. To perform accurate evaluations, the power output of the low-pressure Hg lamp employed in the experiments was carefully measured under the operating conditions.

Table 1
Lamp emission models commonly employed in the simulations of the radiation field in photoreactors.

Type	Name	Abbreviation	Characteristics	Reference
Multiple point source	Multiple point source summation	MPSS	The lamp is modeled as a finite number of emission points equally spaced along the lamp axis.	[20]
	Multiple segment source summation	MSSS	The lamp is modeled as a series of differential cylindrical segments. The radiation is emitted normal to the cylinder surface and decreases with the cosine of the emission angle.	[17,21]
Line source	Spherical emission	LSSE	The lamp is modeled as a line emitting radiation isotropically.	[22]
	Diffuse emission	LSDE	The lamp is modeled as a line emitting radiation diffusely (following the cosine law).	[23]
	Spherical sources	LSSS	The lamp is modeled as a series of differential spheres where the light is generated at the center. Only the component of radiation which is normal to the lamp walls is transmitted.	[18]
Extensive source	Superficial diffuse emission	ESDE	The lamp is modeled as a perfect cylinder. Radiation is diffusely emitted by point emitters uniformly distributed on the lamp surface.	[24]
	Volumetric emission	ESVE	The lamp is modeled as a perfect cylinder. Radiation is isotropically emitted by point emitters uniformly distributed inside the lamp volume.	[25]

2. Experimental

2.1. Far-field evaluation

Several lamp emission models were evaluated against far-field irradiance measurements for a low-pressure Hg lamp (arc length = 277 mm, tube diameter = 15 mm, nominal UV output at 254 nm = 5.7 W, GPH357T5L/4P, Light Sources Inc.) running in air at 22 °C. The actual UV output of the lamp was first determined using the goniometric method (i.e., a series of irradiance measurements in a plane containing the lamp and along an arc scribed at a fixed radius from the center of the lamp) described by the USEPA [33]. Fig. 1 shows a schematic representation of the experimental setup utilized for this test. The irradiance was measured at different radial angles using a calibrated research radiometer (IL1700, SED240 detector, NS254 filter, International Light) once the lamp reached steady emission. The radius from the center of the lamp to the radiometer detector was 1 m, and the readings were recorded rotating the lamp around its transverse axis from 0° to 345° in 15° increments, while the radiometer was kept static. The lamp was then rotated 90° around its longitudinal axis and the measurement process was repeated. Assuming that the emission of the lamp was symmetrical, eight different measurements for each of the angles in the interval from 0° to 90° (0 to $\pi/2$) were obtained.

The power output of the lamp (P) was calculated using the following equation:

$$P = 4\pi R^2 \int_0^{\pi/2} E(\theta)\, \cos\theta \, \mathrm{d}\theta \quad (2)$$

where R is the distance from lamp center to the detector, θ is the angle of the detector from the normal axis of the lamp, and $E(\theta)$ is the irradiance as a function of θ. The integral in Eq. (2) was solved numerically.

The determined UV output and the dimensions of the lamp were fed into different emission models and the irradiances at the same measurement points were predicted. A comparison of the model predictions against the experimental data was performed.

2.2. Near-field evaluation

The near-field evaluation was performed using an annular reactor in which both tubes were made of quartz (inner tube: 23 mm OD/20 mm ID, outer tube: 50 mm OD/46 mm ID, quartz type GE 124, CANSCI Glass Products Ltd.). A schematic with the details of the experimental setup is presented in Fig. 2. This setup allowed measuring the irradiance at specific axial locations around the reactor's outer wall using a chemical actinometer that ran inside a PVC annular jacket (Fig. 2(c)). The PVC annular jacket dimensions were 25.4 mm width, 102 mm OD and 54 mm ID. The actinometer solution run inside a 13 mm wide × 7 mm deep channel formed between the quartz tube and the jacket inner wall. This space was sealed by two o-rings which also allowed moving the jacket to different positions along the reactor. The irradiance measurements were performed on the surface of ~5 mm wide gaps (windows) created on the outer tube wall using several layers of electrical tape (3 M) (see Fig. 2(b)). These measurement windows were located ±5, ±11, ±13 and ±14 cm from the center of the lamp. For calculating the area of each window, the gap widths were carefully measured at several points along the tube circumference using an electronic digital calliper (General, No. 147). The experimental setup also allowed running water with different transmittances and at constant temperature through the annular space of the reactor. In this study, water with 98% UV transmittance and at 22 °C was circulated at a flow rate of 4 L/min in the system. As a safety measure, the reactor's outer tube was covered with black construction paper during the experimental runs.

The actinometer used in this investigation was potassium ferrioxalate solution (0.02 M) prepared and utilized as described by Murov et al. [35]. This actinometer has the advantage that its quantum yield is relatively insensitive to radiation flux [35], making it suitable for near-field measurements. All the chemicals employed were ACS certified, obtained from Fisher Scientific, and used as

received. The same low-pressure Hg lamp used in the far-field tests was employed in these experiments.

The experimental runs were carried out as follows. While running water in the reactor annulus, the UV lamp was placed inside the quartz sleeve (inner tube) and turned on. At least 20 min were given for the system to stabilize and for the lamp to reach steady emission. Following that, 500 mL of actinometric solution were circulated through the PVC jacket at 4 L/min and samples were taken from the container beaker at different time intervals. The concentration of Fe^{2+} was measured via UV spectrophotometry at 510 nm (Carry 100 UV–Visible spectrophotometer, Varian) and the irradiance was calculated [35,36] as

$$E = \frac{4.72 \times 10^5 \cdot V_T}{\Phi \cdot \pi d_o w} \cdot \frac{dC_{Fe^{2+}}}{dt} \cdot 0.89 \quad (3)$$

where V_T is the total volume of actinometric solution, Φ is the quantum yield of potassium ferrioxalate at 254 nm, d_o is the external tube outer diameter, w is the irradiated window width, $dC_{Fe^{2+}}/dt$ is the slope obtained from the linear regression of Fe^{2+}-concentration versus time data, 4.72×10^5 is a factor to convert Einstein to Joule (valid only for 254 nm radiation), and 0.89 is a correction factor for deducting the contributions made by the lamp emitting radiation at wavelengths other than 254 nm [37]. The quantum yield used in the calculations was $\Phi = 1.41$ in accordance with a recent study by Goldstein and Rabani [38].

The power output of the lamp operating inside the annular reactor was verified using a method adapted from Robinson [34] in which the short sleeve section was substituted by a section of annular reactor. Details on the adapted method and equipment setup are available in the Supplementary material.

Simulation of the radiation field in the annular reactor was performed using the estimated power output of the lamp and different emission models. The simulation results were evaluated against the irradiance measurements.

3. Radiation field model

3.1. Solving the governing equation

The RTE was solved using the FV method programmed in commercial CFD code Fluent® 6.3.26. This method considers the RTE in the direction $\vec{s}$ as a field equation [5]. Eq. (1) is rewritten and solved as:

$$\nabla \cdot (I(\vec{r}, \vec{s})\vec{s}) + (\kappa + \sigma) I(\vec{r}, \vec{s}) = \kappa n^2 \frac{\sigma_{S-B} T^4}{\pi} + \frac{\sigma}{4\pi} \int_{4\pi} I(\vec{r}, \vec{s}\,') p(\vec{s}\,' \to \vec{s})\, d\Omega' \quad (4)$$

where n is the refractive index, σ_{S-B} is the Stefan–Boltzmann constant (5.672×10^{-8} W m^{-2} K^{-4}), and T is the absolute temperature of the medium. Inside the photoreactor there is no UV radiation emission (generation), except for the lamp. Therefore, the source term (first term in the right-hand side of Eq. (4)) was almost inactivated by setting the computational domain temperature (everywhere except the lamp) to 1 K (minimum temperature allowed by Fluent). The definition of the UV radiation emitted by the lamp is described in section 3.2. Note that because the domain zone temperatures are set equal to constant values (1 K), this approach can only be used for the simulation of systems that can be treated as isothermal reactors (this is usually the case for photocatalytic reactors). However, for cases where the reacting system is not isothermal, the emission terms of the different domain zones can be defined utilizing a sub-program (a user defined function in Fluent).

The segregated steady-state solver was used for solving the governing equation. An angular discretization of 40 divisions was used. This number was found to be sufficient to avoid the appearance of the "ray effect" [9]. To overcome control angle overhang, a 1×1 pixelation was used [9]. Due to the symmetry of the studied system, 2D axisymmetric simulations were performed. This approach was preferred since it is much less computationally intensive than 3D simulations. Moreover, little difference (<1%) between 2D and 3D solutions was found in preliminary evaluations. Second order upwind discretization scheme was employed. Convergence of the numerical solution was assured by monitoring the scaled residuals to a criterion of at least 10^{-6}. Additionally, the variation of fluence rate at several points (or irradiance at different surfaces) of the computational domain was used as the indicator of convergence.

Commercial mesh generator Gambit® 2.2.30 was used to create the grid. Structured quadrilateral cells were used to discretize the physical domain. Boundary-layer mesh was setup at the lamp wall where high radiation gradients occur. The utilized grids were verified to give mesh-independent results. In the simulations performed, approximately 20,000 cells were used.

3.2. Lamp emission models and boundary conditions

In the present investigation, the lamp (radiation source) was part of the computational domain. As discussed in the introduction, there are different ways to model the radiation emission of a lamp. Therefore, different approaches were taken to simulate these emission patterns using the CFD software. For the ESVE, the plasma volume (a cylinder) was defined as a fluid or solid continuum. The lamp emission power was defined by the absorption coefficient, the refractive index, and the temperature of the plasma (see source term in Eq. (4)). The ESVE model assumes that the absorption coefficient is zero [25], even though a small value was needed to be defined (e.g., 0.01 m^{-1}). The refractive index was assumed as 1 given that the lamp is filled with an inert gas and Hg at a very low concentration. The temperature was then determined using the following iterative procedure: a first guess of the temperature was set in the model and the simulation was run; the power output coming out of the lamp envelope was checked; if the obtained value disagreed with the desired one, a new plasma temperature was calculated realizing that the power output is proportional to T^4. The lamp envelope was defined as a zero-thickness, semi-transparent, fully specular wall (diffuse fraction = 0); the cylinder end caps were semi-transparent, fully diffused walls that absorbed all the incident radiation. Complete radiation absorption at these walls was set in Fluent assigning a thickness (e.g., 2 mm) and a high absorption coefficient (e.g., 10,000 m^{-1}).

The ESDE was simulated the same way as the ESVE, except that the lamp envelope needed to be set as a purely diffused wall (diffuse fraction = 1). Another alternative to simulate the ESDE was defining only the external walls of the lamp (lamp = hollow cylinder). In this case, the lamp envelope was a semi-transparent, purely diffused exterior wall with external irradiation. The external irradiation was calculated dividing the power output of the lamp by the envelope surface area. The cylinder end caps were semi-transparent, fully diffused walls that absorbed all the incident radiation.

The LSSE and LSDE were simulated in the same way as the ESVE and ESDE, respectively; except that the diameter of the lamp cylinder was made so small that a linear approximation could be achieved. In the simulations performed, the ratio between the lamp length and diameter was 1385. The LSSS model is mathematically identical to LSDE, except for a $\pi/4$ factor. Thus, the LSSS model was simulated as the LSDE, but with the power emission reduced by $\pi/4$.

Additional lamp emission models were evaluated in this study; however, they were basically modifications of the ESDE and ESVE models in which reflection/refraction/absorption effects at the quartz envelope, and/or a higher photon absorption/re-emission

Table 2
Refractive indexes (n) and absorption coefficients (κ) used in the simulations.

Material	n	κ (m^{-1})
Lamp plasma	1.00	0.01[a]/191[b]
Air	1.00	0
Water	1.38[c]	2.02[d]
GE 124 Quartz	1. 52[e]	22[f]
Actinometer	1.38[g]	0[h]

[a] Used for transparent plasma.
[b] Used for absorbing plasma Ref. [15].
[c] Ref. [39].
[d] Calculated for water with 98% transmittance.
[e] Refs. [40,41].
[f] Ref. [41].
[g] The same value of water was assumed.
[h] Assumed zero because the absorption effect was not modeled.

in the Hg plasma were included. Reflection/refraction/absorption at the quartz envelope was considered in Fluent by giving some thickness (e.g., 1 mm) to the envelope wall [5]. Higher photon absorption/re-emission in the Hg plasma was accomplished by increasing the photon absorption coefficient. It is important to mention that since these changes caused modifications in the radiation emission inside the lamp, the plasma temperature needed to be checked and properly adjusted every time to guarantee the desired lamp output.

The quartz sleeve and the external quartz tube were simulated as solid continuums enclosed by zero-thickness, semi-transparent, fully specular walls. This was done to better simulate radiation refraction and propagation inside these walls, and also because the thickness of the walls were considerable when compared to the radial length of the computational domain (~14%). Both, the air surrounding the lamp and the water inside the annulus were defined as fluid continuums (solid continuum is also adequate if the fluid is static). The annular jacket with the actinometric solution was also included in the computational domain. The actinometer was defined as a fluid continuum and the jacket walls were zero-thickness, opaque, fully diffused, non-reflective walls. This was also the case for the external side walls of the reactor. Non-reflectivity of opaque walls was defined making the emissivity equal to 1 [5,9]. Due to the symmetry of the system, a symmetry boundary condition (BC) was imposed at the center of the reactor. The computational domain of the annular reactor simulated in the present work is shown in the 2D geometrical model of Fig. 3.

3.3. Optical properties

The refractive index and the absorption coefficient are the optical properties of the materials necessary for the simulations. Table 2 lists the values for these two properties for each of the materials present in the simulations.

4. Results and discussion

4.1. Verification of the lamp emission models

Before starting to evaluate the radiation models against the experiments where complex optical effects take place, a verification of the emission models was performed for the simple case of an emitting lamp running in air (5.7 W power output, 277 mm arc length, 15 mm diameter). The lamp emission models were verified against analytical (LSSE, LSDE and LSSS) or numerical solutions (ESVE and ESDE) of the corresponding mathematical models. The agreement between the model predictions and the analytical/numerical solutions of the mathematical models was excellent for both, irradiance and fluence rate. These results confirm the suitability of using the proposed approach for simulating different lamp emission models. A detailed description of the model verifications and the obtained results are available in the Supplementary material.

4.2. Far-field evaluation

Fig. 4 shows the irradiance values obtained using the goniometric method described in section 2.1. The irradiance measurements presented a cosine-like functionality, very similar to the ones reported in other investigations [33,42]. A cosine response is distinctive of diffused (lambertian) emitters; thus, these results suggest that the lamp has an emission pattern similar to that of a diffused emitter. Using Eq. (2), the power output of the lamp was calculated as 4.5 W.

The determined lamp power output was fed into different lamp emission models to predict the irradiance at the locations where the goniometric measurements were performed. As a first stage in the analysis, the traditional LSSE, LSDE, LSSS, ESDE and ESVE models were evaluated. Additional details of these calculations are presented in the Supplementary material where the mathematical deduction of the model obtained for the case of the LSSE emission model is presented. As seen in Fig. 4(a), irradiance predictions based on the LSSE and ESVE models did not match the experimental data at all. These models predicted that the irradiance at the sensor would gradually rise as the lamp is rotated; and in the case of the ESVE it would sharply drop to zero as the angle reaches 90°. This same behavior was reported by other researchers [42] for the LSSE model. Moreover, calculations made using other systems with different L/R ratios verified that these are general model behaviors and that the irradiance rise is steeper as L/R increases. The model behaviors are the consequence of assuming isotropic emission from the lamp emitting elements. With this assumption, the radiation emitted by each element towards the sensor is the same irrespective of the sensor position. In addition, the radiometer sensor gets closer to the lamp as the angle increases in the goniometric measurements. These results clearly indicate that LSSE and ESVE do not model properly the emission pattern of the lamp, and that they should not be utilized for far-field predictions. LSSS model predictions showed cosine functionality; however, the irradiance predictions were $\sim\pi/4$ lower than the experimental values. LSSS predictions were lower because this model is not energy conservative, i.e., the integration of irradiance over an enclosing surface around the lamp does not yield the total power output of the lamp; it only yields $\pi/4$ of the lamp output. In the development of this model, the irradiance of the MPSS is simply multiplied by the cosine function, resulting in a lower emitted power of the differential elements [42]. The same analysis applies to the MSSS, since MSSS is mathematically identical to the LSSS in the limit as the number of point sources becomes infinite. LSSS and MSSS are therefore not recommended to be utilized as emission models. On the other hand, LSDE and ESDE predictions had a much closer agreement with the experimental measurements. For $0 < \theta < 50$, the estimated and measured values agreed quite well and for $50 < \theta < 90$, a small overprediction was found. These models consider that radiation is diffusely emitted by the lamp, implying that the real lamp emission must be to some extent similar to that of a lambertian emitter. Evidence of cosine-liked emission from a low-pressure mercury UV lamp was also obtained by André et al. [43] who made irradiance measurements very close to the lamp envelope wall using a fiber optic.

Even though the irradiance predictions of LSDE and ESDE were not completely accurate for all the directions around the lamp, their overall performance was good and acceptable. As a matter of fact, a formula based on the LSDE model has been recently proposed [44] to be used in a standard method for calculating the total UV output

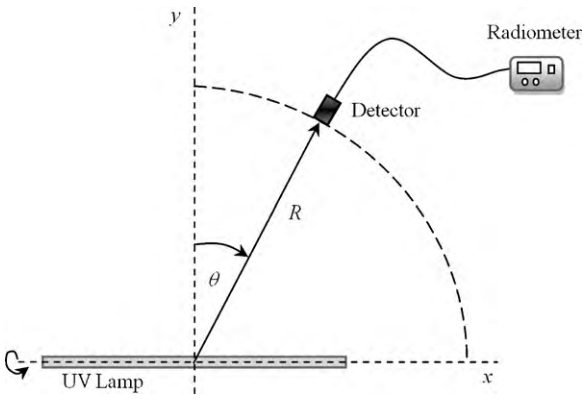

Fig. 1. Schematic of the experimental setup utilized for performing far-field evaluation of lamp emission models.

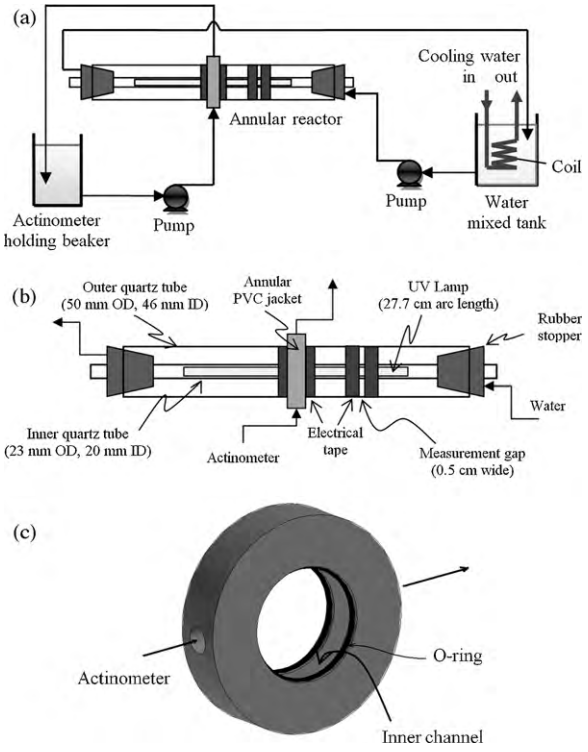

Fig. 2. Schematic of the equipment and experimental setup employed for the near-field irradiance measurements. Details of (a) experimental setup (b) the annular reactor, and (c) annular PVC jacket.

of a monochromatic lamp. According to this method, the irradiance at a normal distance from the center of a lamp is measured using a radiometer. The power output (for $y \geq 2L$) is calculated using the

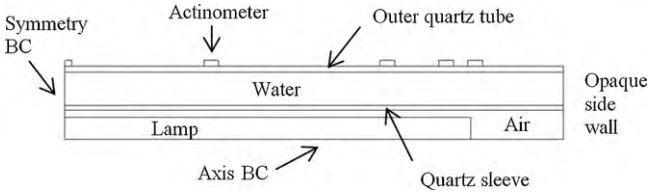

Fig. 3. 2D geometrical model of the annular reactor utilized in the near-field evaluation study. Boundary conditions (BC) and continuums of the computational domain are shown.

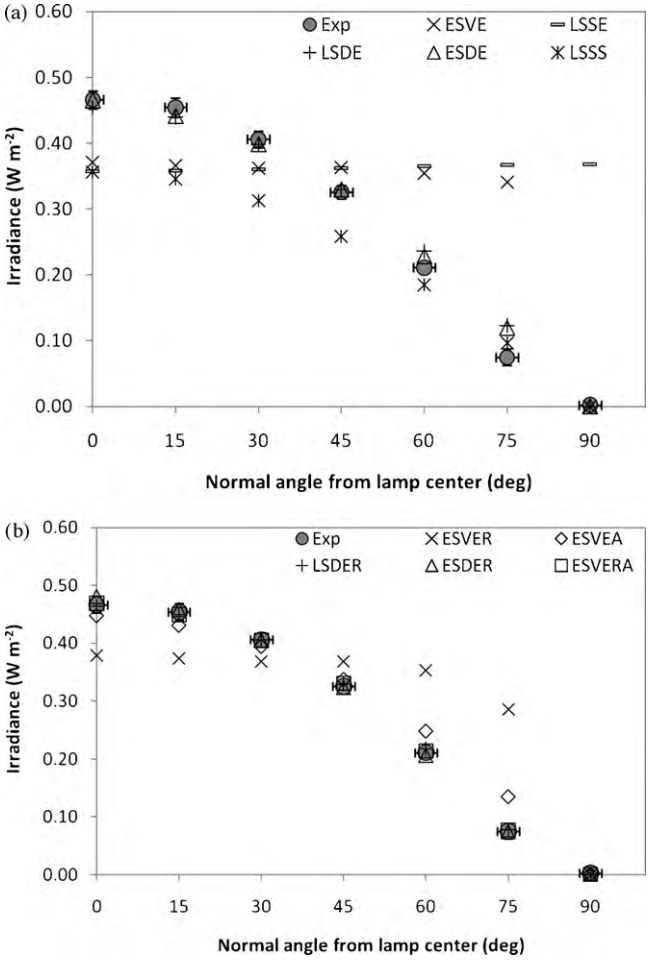

Fig. 4. Goniometric irradiance measurements obtained 1 m away from the lamp center (Exp) and their comparison with different lamp emission model predictions: (a) LSSE, LSDE, LSSS, ESDE, and ESVE, (b) LSDER, ESDER, ESVER, ESVEA, and ESVERA. The error bars represent the 95% confidence interval calculated for eight measurements.

Keitz formula [45]:

$$P = \frac{E2\pi^2 yL}{2\alpha + \sin 2\alpha} \quad (5)$$

where y is the normal distance from the lamp center, L is the lamp arc length, α is the half angle subtended by the lamp at the sensor position (i.e., $\tan\alpha = L/(2y)$). On the other hand, an older method based on the LSSE model, which assumes that at considerable distance the lamp can be taken as a point source emitter ($P = 4\pi y^2 E$) has

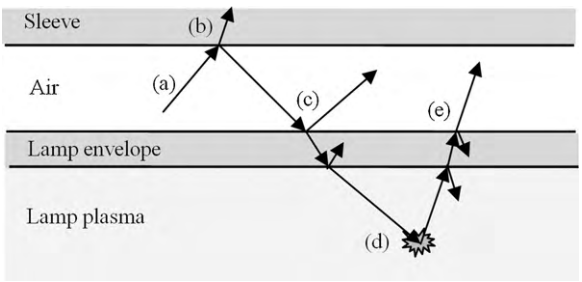

Fig. 5. Schematic representation of the phenomena and interactions taking place when a lamp is operated inside of a quartz sleeve: (a) radiation coming from the lamp, (b) reflection and refraction at the quartz sleeve, (c) reflection and refraction at the lamp envelope, (d) absorption and re-emission of photons by Hg atoms, and (e) radiation re-escaping from the lamp envelope.

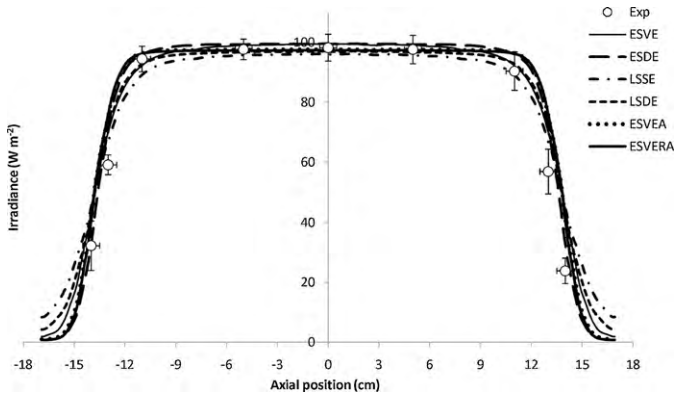

Fig. 6. Irradiance measured at different positions of the reactor outer wall compared with the predictions of different lamp emission models. The error bars represent the 95% confidence interval obtained with triplicate runs.

been proven to considerably overestimate (~20%) the UV output of the lamp [46].

To analyze if better model predictions could be achieved, the LSDE, ESDE, and ESVE models were modified to account for radiation reflection, refraction and absorption at the lamp quartz envelope (these modified models were abbreviated as LSDER, ESDER, and ESVER, respectively). These effects were included in the FV-based model assigning a 1 mm thickness to the envelope wall and adjusting the plasma temperature to obtain 4.5 W power output. As can be seen in Fig. 4(b), the incorporation of reflection, refraction and absorption to LSDE and ESDE made the model predictions fit the experimental data very well; this not being the case for ESVE. These results suggest that radiation is diffusely emitted from a thin layer of plasma next to the inner envelope wall, after which it suffers reflection, refraction and absorption at the quartz envelope. Computations performed for LSDE in which only reflection was incorporated into the model demonstrated that this effect accounts for practically all the correction given to the model predictions.

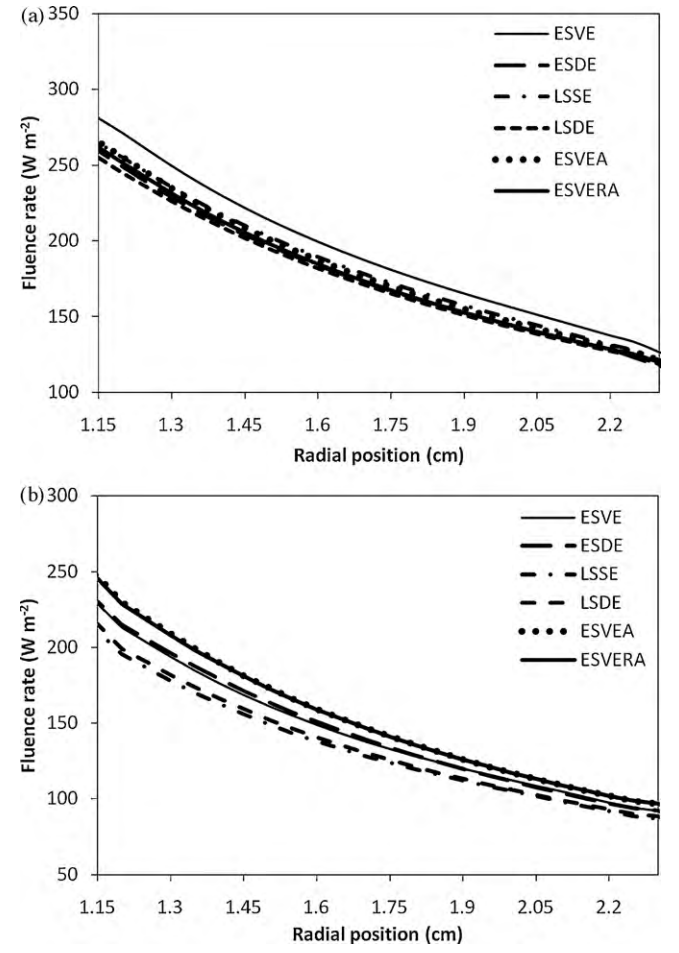

Fig. 7. Fluence rate profiles along the radial coordinate in the annular space as computed using different lamp emission models. The results correspond to the center of the reactor.

The results obtained here can be explained by analyzing the physical processes occurring inside a low-pressure Hg lamp. It is well known that photons are emitted all over the lamp plasma volume. However, since this emission process is reversible, photons can be absorbed and isotropically re-emitted by another mercury atom before escaping the lamp envelope [47]. This absorption/re-emission process is significant due to the high absorption coefficient of the Hg plasma, and it becomes more important in those directions implying a longer pathway for the photons (i.e., for increasing θ values). As a consequence, compared to that from inside parts of the plasma, higher emission rates occur near the walls of the lamp, and diffused emission takes place. Based on this analysis, the ESVE model was modified to account for the absorption/re-emission effect (model abbreviation: ESVEA). This modification was made in the computational model by setting a high absorption coefficient for the lamp plasma (191 m^{-1} as reported by Imoberdorf et al. [15]), and again, adjusting the plasma temperature to obtain 4.5 W power output. As it can be seen in Fig. 4(b), the irradiance predictions obtained with the ESVEA model were practically the same as the ones obtained with LSDE and ESDE. This result proves that the absorption/re-emission process can adequately explain the diffused radiation emission observed in the experimental measurements. Moreover, when reflection, refraction, and absorption at the lamp envelope were included to the ESVEA model (model abbreviated as ESVERA), the irradiance predictions fitted the experimental measurements fully (see Fig. 4(b)). The ESVERA model coincides fundamentally with the model proposed and evaluated by Imoberdorf et al. [15] for multi-lamp, homogeneous photoreactors.

The ESVERA emission model shows great potential for being applied in CFD simulations. The model is very easy to set up and its far-field irradiance predictions agreed fully with the measurements. As a second alternative, the ESDE should be considered.

4.3. Near-field evaluation

Before evaluating the irradiance prediction capabilities of different emission models in the near-field region, the power output of the lamp while operating inside the annular reactor was verified. For this, the method presented in section 2.2 and fully described in the Supplementary material was implemented. The obtained results indicated that under the experimental conditions the lamp output was the same (within the experimental error estimated at 5%) as when the lamp was running in air. This result can be explained by the fact that the generated heat in the annular reactor was removed by the water of the same temperature as ambient air (22 °C). This situation propitiates comparable heat transfer conditions in both systems resulting in similar lamp temperatures and consequently, the same power outputs.

The temperature of the water in the reactor was varied (5 – 35 °C) to study its effect on the lamp power output. Different operating water temperatures produced variations of up to 15% in the lamp output corroborating the importance of performing the determination of the lamp UV output under the actual operating conditions of the reactor. The detailed results can be found in the Supplementary material.

When a lamp is operated inside a quartz sleeve, there are important phenomena that need to be taken into account for the simulation of radiation distribution. These phenomena are schematically illustrated in Fig. 5. From the radiation coming from the lamp and reaching the quartz sleeve, a fraction is transmitted through the quartz wall and the other part is reflected backwards. Part of this reflected radiation reaches the lamp envelope where a fraction suffers reflection again; however, the rest of radiation re-enters the lamp body. These photons that re-enter the lamp body are absorbed and re-emitted multiple times by Hg atoms until they finally escape the lamp [15]. Consequently, since each photon that re-enters will exit the lamp again, the net photon emission of the lamp remains constant. When simulating this system using the developed FV-based model, the part of radiation that re-enters the lamp and is absorbed by the Hg plasma is correctly taken into account, but the effect of re-emission of these absorbed photons is not considered in the governing equation and thus, not computed. Nonetheless, this additional generation of photons (due to re-emission) can be simulated by simply increasing the plasma temperature until the corresponding net power output is met. Following this approach, a net lamp power output of 4.5 W was assured in all the annular reactor simulations performed.

A corollary of the previous analysis on the interaction between the quartz sleeve and the lamp is that practically all the radiation that is generated in the lamp will end up being transmitted into the sleeve wall; there is consequently no "loss" of radiation because of reflection at the air/quartz sleeve interface. The reflected radiation re-enters the lamp, is absorbed and subsequently re-emitted towards the sleeve; or if it misses the lamp, it will continue travelling until it reaches the sleeve at some other position. This results from the conservation of radiative energy in the lamp-sleeve control volume. Under this approach, the use of radiation models that deduct the reflected radiation at the air/sleeve interface might result in underprediction of the irradiance (or fluence rate) inside the photoreactor.

Using the quartz tube annular reactor and the actinometer solution running inside the annular PVC jacket, the irradiance at different axial positions was determined (Fig. 6). It is evident that the studied lamp had symmetrical emission and that the irradiance at the wall had a flat profile within ~70% of the irradiated area ($-11\,\text{cm} < x < +11\,\text{cm}$), followed by a steep decrease in the region $12\,\text{cm} < |x| < 15\,\text{cm}$.

Fig. 6 also shows the predicted irradiance at the reactor outer tube wall using the FV-based model with different radiation emissions and the experimentally determined lamp power output. Analyzing the region with practically flat irradiance profile ($-11\,\text{cm} < x < +11\,\text{cm}$), it can be noticed that the prediction of the different models were somewhat similar. Due to the experimental error (~5%) associated with the actinometric determinations in that zone, it is not possible to affirm whether one particular model performs better than the others. Nonetheless, it is interesting to see how exactly ESVERA and ESVEA predicted the average of the experimental measurements. In the region of steep decrease of the irradiance ($12\,\text{cm} < |x| < 15\,\text{cm}$), all the models somehow overpredicted the irradiance at the tube wall. Note that in this region the experimental error was much larger (~15%). The models that predicted the steepest decrease and thus the closest agreement with the experimental data were ESVERA, ESVEA, and ESDE. This latter result is consistent with the far-field evaluation since these three models showed good irradiance predictions in high-normal-angle propagation directions.

While the irradiance profiles predicted using LSSE and ESVE were somehow in fair agreement with the experimental data, their far-field predictions fell far away from the experimental points. This result demonstrates that in the region close to the lamp, the radiation emission pattern (isotropic or diffused) has little effect on the irradiance prediction profiles. Nevertheless, this is not the case for other radiation field variables such as the fluence rate. Fig. 7 shows the fluence rate profiles computed by different lamp emission models along the radial coordinate in the annular space at the center and one side ($x = 13\,\text{cm}$) of the reactor. As can be seen, significant prediction differences can be found among the different models. These results have important implications for the simulation of photoreactors with volumetric reactions, since photochemical reaction rates are determined by the local fluence rate.

The models that assumed (or resulted in) diffused radiation emission (LSDE, ESDE, ESVEA, and ESVERA) were the ones that showed better overall irradiance prediction capabilities. In other investigations [15–17,21,23,24,36], diffused emission models have also shown good results not only in terms of irradiance, but also fluence rate prediction accuracy. In few of those studies [17,21], the authors utilized the MSSS model in the radiation distribution calculations. As mentioned before, this model reduces the radiation output of the lamp by $\pi/4$. However, the two studies referred above have used the method based on LSSE (which overestimates the real output in about $\pi/4$) for estimating the lamp output. As a consequence, the predictions they obtained are equivalent to LSDE model predictions.

The annular reactor simulations performed in all the previous evaluations considered the quartz sleeve and the outer tube as solid continuums enclosed by zero-thickness, semi-transparent, fully specular walls. To analyze if the model geometry could be simplified without sacrificing prediction accuracy, a simulation in which the quartz sleeve was defined as a regular BC wall was performed. The obtained irradiance predictions were practically the same for both systems, so for future works, it is recommended to treat the sleeve as a regular BC wall. Full details of this evaluation can be found in the Supplementary material.

5. Conclusions

A computational radiation field model based on the finite-volume method was developed for simulating the irradiance in single-phase annular photoreactors. As part of the model, a CFD-based approach for modeling lamp radiation emission was proposed. Under this approach, the lamp is included in the computational domain and the lamp plasma emission is simulated by defining proper physical properties and boundary conditions, allowing for different emission patterns to be defined in the model. For developing the radiation model, several lamp emission models were evaluated against near- and far-field irradiance measurements. The main conclusions withdrawn from this investigation were:

- The far-field evaluation showed that LSSE, LSSS and ESVE model predictions were in complete disagreement with the experimental data. Thus, these models are not recommended for far-field predictions. On the other hand, diffused emission models (LSDE and ESDE) predicted fairly well the irradiance distribution around the lamp. Moreover, incorporating reflection/refraction/absorption effects at the lamp quartz envelope to these diffused models allowed for even better far-field irradiance predictions.
- When the high photon absorbance/re-emission effect produced by the Hg vapor was considered in the ESVE model (ESVEA model), it was able to explain the diffused emission behavior of the lamp. Moreover, adding reflection/refraction/absorption effects at the lamp quartz envelope (ESVERA model) resulted in an excellent match between predictions and experimental data.
- Near-field evaluation revealed that the radiation emission pattern (isotropic or diffused) has little effect on the irradiance

prediction close to the lamp. However, important differences were observed for the fluence rate predictions. Even though the predicted irradiance profile using different emission models was somehow similar, ESDE, ESVEA, and ESVERA presented the closest agreement with the experimental data.

- ESVERA is a promising emission model to be incorporated in integrated models, such as the CFD-based simulations of photoreactors, particularly immobilized photocatalytic reactors. The model is very easy to set up, it comprises the main physical phenomena occurring in the lamp, it allows taking into account important lamp-sleeve interactions, and it shows excellent agreement with near- and far-field experimental data.
- Experiments obtained for the lamp operating inside the quartz sleeve of the annular reactor demonstrated the strong effect of surrounding temperature on the lamp power output. Consequently, to perform accurate simulations, it is essential to obtain and use a real estimate of the lamp power output under the actual operating conditions in the reactor.

Acknowledgements

The authors acknowledge Dr. Gustavo Imoberdorf for his valuable input and discussions, and the Natural Sciences and Engineering Research Council of Canada (NSERC) for financial support. J. Esteban Durán also thanks the support received from Universidad de Costa Rica.

Appendix A. Supplementary data

Supplementary data associated with this article can be found, in the online version, at doi:10.1016/j.jphotochem.2010.07.027.

References

[1] J.M. Herrmann, Heterogeneous photocatalysis: state of the art and present applications, Top. Catal. 34 (2005) 49–65.
[2] M.R. Hoffmann, S.T. Martin, W. Choi, D.W. Bahnemannt, Environmental applications of semiconductor photocatalysis, Chem. Rev. 95 (1995) 69–96.
[3] D.F. Ollis, C. Turchi, Heterogeneous photocatalysis for water purification: contaminant mineralization kinetics and elementary reactor analysis, Environ. Prog. 9 (1990) 229–234.
[4] A.E. Cassano, C.A. Martin, R.J. Brandi, O.M. Alfano, Photoreactor analysis and design: fundamentals and applications, Ind. Eng. Chem. Res. 34 (1995) 2155–2201.
[5] Fluent-Inc., FLUENT 6.3 User's Guide, Lebanon, 2006.
[6] M.N. Ozisik, Radiative Transfer and Interactions with Conduction and Convection, Wiley, New York, 1973.
[7] M.G. Carvalho, T.L. Farias, Modelling of heat transfer in radiating and combusting systems, Trans. IChemE: Part A 76 (1998) 175–184.
[8] V. Pareek, S. Chong, M. Tadé, A.A. Adesina, Light intensity distribution in heterogenous photocatalytic reactors, Asia-Pac. J. Chem. Eng. 3 (2008) 171–201.
[9] V.K. Pareek, A.A. Adesina, Light intensity distribution in a photocatalytic reactor using finite volume, AIChE J. 50 (2004) 1273–1288.
[10] V.K. Pareek, S.J. Cox, M.P. Brungs, B. Young, A.A. Adesina, Computational fluid dynamic (CFD) simulation of a pilot-scale annular bubble column photocatalytic reactor, Chem. Eng. Sci. 58 (2003) 859–865.
[11] V. Pareek, Light intensity distribution in a dual-lamp photoreactor, Int. J. Chem. React. Eng. 3 (2005), Article A56.
[12] F.J. Trujillo, T. Safinski, A.A. Adesina, CFD Analysis of the radiation distribution in a new immobilized catalyst bubble column externally illuminated photoreactor, J. Sol. Energy Eng. 129 (2007) 27–36.
[13] F.J. Trujillo, I. Lee, C. Hsu, T. Safinski, A.A. Adesina, Hydrodynamically-enhanced light intensity distribution in an externally-irradiated novel aerated photoreactor: CFD simulation and experimental studies, Int. J. Chem. React. Eng. 6 (2008), Article A58.
[14] F. Denny, J. Scott, V. Pareek, G.D. Peng, R. Amal, CFD modelling for a TiO_2-coated glass-bead photoreactor irradiated by optical fibres: photocatalytic degradation of oxalic acid, Chem. Eng. Sci. 64 (2009) 1695–1706.
[15] G.E. Imoberdorf, F. Taghipour, M. Mohseni, Radiation field modeling of multilamp, homogeneous photoreactors, J. Photochem. Photobiol. A 198 (2008) 169–178.
[16] O.M. Alfano, R.L. Romero, A.E. Cassano, Radiation field modelling in photoreactors – I. Homogeneous media, Chem. Eng. Sci. 41 (1986) 421–444.
[17] D. Liu, J. Ducoste, S. Jin, K. Linden, Evaluation of alternative fluence rate distribution models, J. Water Supply Res. Technol. AQUA 53 (2004) 391–408.
[18] R. Tsekov, P.G. Smirniotis, Radiation field in continuous annular photocatalytic reactors: role of the lamp finite size, Chem. Eng. Sci. 52 (1997) 1667–1671.
[19] H.A. Irazoqui, M.A. Isla, A.E. Cassano, Simplified extense source model for photoreactor analysis and design, Ind. Eng. Chem. Res. 39 (2000) 4260–4271.
[20] S.M. Jacob, J.S. Dranoff, Light intensity profiles in a perfectly mixed photoreactor, AIChE J. 16 (1970) 359–363.
[21] R.O. Rahn, J. Bolton, M.I. Stefan, The iodide/iodate actinometer in UV disinfection: determination of the fluence rate distribution in UV reactors, Photochem. Photobiol. 82 (2006) 611–615.
[22] E.R. Blatchley III, Numerical modelling of UV intensity: application to collimated-beam reactors and continuous-flow systems, Water Res. 31 (1997) 2205–2218.
[23] T. Akehata, T. Shirai, Effect of light-source characteristics on the performance of circular annular photochemical reactor, J. Chem. Eng. Jpn. 5 (1972) 385–391.
[24] T. Yokota, T. Iwano, T. Tadaki, Light intensity in an annular photochemical reactor, Kagaku Kogaku Ronbunshu 2 (1976) 298–303.
[25] H.A. Irazoqui, J. Cerdá, A.E. Cassano, Radiation profiles in an empty annular photoreactor with a source of finite spatial dimensions, AIChE J. 19 (1973) 460–467.
[26] Y. Quan, S.O. Pehkonen, M.B. Ray, Evaluation of three different lamp emission models using novel application of potassium ferrioxalate actinometry, Ind. Eng. Chem. Res. 43 (2004) 948–955.
[27] M. Salaices, B. Serrano, H.I. de Lasa, Experimental evaluation of photon absorption in an aqueous TiO_2 slurry reactor, Chem. Eng. J. 90 (2002) 219–229.
[28] S. Jin, K.G. Linden, J. Ducoste, D. Liu, Impact of lamp shadowing and reflection on the fluence rate distribution in a multiple low-pressure UV lamp array, Water Res. 39 (2005) 2711–2721.
[29] B.F. Severin, P.F. Roessler, Resolving UV photometer outputs with modeled intensity profiles, Water Res. 32 (1998) 1718–1724.
[30] L.J. Forney, J.A. Pierson, Photolytic reactors: similitude in Taylor–Couette and channel flows, AIChE J. 49 (2003) 1285–1292.
[31] Ultraviolet Technology of Australasia, The Critical Factors in Ultraviolet Disinfection Systems, 2009, http://www.uvta.com.au/pdf/critical_factors.pdf [accessed 22.11.09].
[32] W. Bahnfleth, J. Lau, P. Kremer, D. Clark, J. Freihaut, Emerging Filter and UV Devices for Energy Efficient IAQ in Commercial Buildings. Volume 2: Germicidal Lamp Testing, Indoor Environment Center, The Pennsylvania State University, 2009.
[33] USEPA, Design Manual: Municipal Wastewater Disinfection, EPA/625/1-86/021, Cincinnati, 1986.
[34] J. Robinson, Determination of the output of a UV lamp running in a quartz sleeve submerged in water, in: World Congress on Ozone and Ultraviolet Technologies, International Ozone Association and International Ultraviolet Association, Los Angeles, 2007.
[35] S.L. Murov, I. Carmichael, G.L. Hug, Handbook of Photochemistry, 2nd ed., Marcel Dekker Inc., New York, 1993.
[36] R.L. Romero, O.M. Alfano, A.E. Cassano, Radiation field in an annular, slurry photocatalytic reactor. 2. Model and experiments, Ind. Eng. Chem. Res. 42 (2003) 2479–2488.
[37] R.O. Rahn, M.I. Stefan, J.R. Bolton, E. Goren, P.S. Shaw, K.R. Lykke, Quantum yield of the iodide-iodate chemical actinometer: dependence on wavelength and concentration, Photochem. Photobiol. 78 (2003) 146–152.
[38] S. Goldstein, J. Rabani, The ferrioxalate and iodide-iodate actinometers in the UV region, J. Photochem. Photobiol. A 193 (2008) 50–55.
[39] I. Thormählen, J. Straub, U. Grigull, Refractive index of water and its dependence on wavelength, temperature and density, J. Phys. Chem. Ref. Data 14 (1985) 933–945.
[40] D.R. Lide, Handbook of Chemistry and Physics, 89th ed, CRC Press, Boca Raton, 2008.
[41] Momentive, http://www.gequartz.com/en/optical.htm [accessed 22.11.09].
[42] M.R. Sasges, A. van der Pol, A. Voronov, J. Robinson, A standard method for quantifying the output of UV lamps, in: World Congress on Ozone and Ultraviolet Technologies, International Ozone Association and International Ultraviolet Association, Los Angeles, 2007.
[43] J.C. André, M. Roger, J. Villermaux, Répartition de la luminière dans un réacteur photochimique de symétrie cylindrique, Chem. Eng. J. 31 (1985) 199–208.
[44] O. Lawal, B. Dussert, C. Howarth, K. Platzer, M. Sasges, J. Muller, E. Whitby, R. Stowe, V. Adam, D. Witham, S. Engel, P. Posy, A. van der Pol, Proposed method for measurement of the output of monochromatic (254 nm) low pressure UV lamps, IUVA News 10 (2008) 14–17.
[45] H.A.E. Keitz, Light Calculations and Measurements, 2nd ed., St. Martin's Press Inc., New York, 1971.
[46] G.E. Whitby, B. Sotirakos, J.R. Bolton, A comparison of two methods for measuring the UV output of low pressure mercury lamps in air, in: World Congress on Ozone and Ultraviolet Technologies, International Ozone Association and International Ultraviolet Association, Boston, 2009.
[47] W.J. Masschelein, Ultraviolet Light in Water and Wastewater Sanitation, Lewis Publishers/CRC Press, Boca Raton, 2002.